ChemistryEurope
Excellence in Chemistry Research Worldwide

Research Article
doi.org/10.1002/ceur.202500104

www.journal.chemistry-europe.org

Advancing Light-Triggered Alkyd Paint Curing: $(Cp)Fe^{II}(naphthalene)](PF_6)$ Catalysts with Enhanced Photosensitivity and Increased Performance in Pigmented Alkyd Paints

Jens Tolboom, Alexis K. Bauer, Johan Bootsma, Jitte Flapper, Michael L. Neidig, and Bas de Bruin*

The class of photoactive complexes $[(Cp)Fe^{II}(arene)]^+$ (Cp = cyclopentadienyl, arene = C_6H_6, C_6H_5;Me) enable light-controlled alkyd paint curing, eliminating the need for anti-skinning agents. While $[(Cp)Fe^{II}(benzene)](PF_6)$ (0.10 wt%) initiates curing under ambient light (116 Lux/1.7 mW/m^2) within 6 h for transparent paints, it is ineffective in dark-colored formulations. Here, we demonstrate that the more photosensitive complexes $[(Cp)Fe^{II}(L)](PF_6)$ (L = naphthalene, 5-methoxynaphthalene, 6-methoxy-naphthalene, 5,8-dimethoxynaphthalene) accelerate curing with lower loadings (0.05 wt%). Due to their higher extinction coefficients and red-shifted adsorption bands, these $[(Cp)Fe^{II}(L)](PF_6)$ catalysts effectively cure dark-pigmented paints. Mössbauer spectroscopy reveals the formation of a high-spin Fe^{II} intermediate as the active species. TD-DFT calculations reveal a redshift in absorption, attributed to a transition from dz^{2}-d_{xy}*/d_{yz}* (arene/naphthalene) to L_{π}-d_{xy}*/d_{yz}* (methoxylated naphthalenes). Excitation of the complexes using wavelengths corresponding to these absorbance bands result in weakening of the Fe^{II}-η^6C_6 bonds, facilitating light-induced dissociation. This advancement enhances latency originating from photoactivation while expanding applicability to pigmented systems.

1. Introduction

Light-triggered catalysts play a crucial role in utilizing light energy to drive chemical transformations. Unlike conventional catalytic processes that typically rely on heat or chemical reactants to initiate reactions, photocatalysis harnesses photons to activate catalysts and facilitate reactions under mild conditions.[1–4] Upon light absorption, these catalysts access excited states that lower activation barriers, enabling diverse transformations at ambient temperature and pressure.

To ensure broad applicability, catalysts ideally operate effectively under low solar irradiances as this can vary regionally—from 205 to 250 W m^{-2} at the equator to 115–125 W m^{-2} at mid-latitudes—due to differences in solar angle and atmospheric filtering.[5,6] Specifically designed light-triggered catalysts possess the capability to adjust their catalytic activity upon exposure to this type of light, with the potential to accelerate catalytic rate, or change material properties using photo-switching. This dynamic control has reignited interest in light-triggered polymerizations due to their application in traditional materials such as adhesives and inks, but mainly due to their development in high-tech applications such as 3D-printing and nanotechnology.[7–11] These industries rely heavily on the precise activation of photo-initiators, photoactivated catalysts or photocatalysts to initiate the formation of polymers or cross-links upon exposure to specific light wavelengths.

Iron-based photointitators/catalysts are well explored for photocrosslinking and polymerization. Compounds like **Irgacure 261**,[12] **CFC**,[13] and **FC-NP** (**Scheme 1**)[14,15] have been known for their role in cationic ring opening (photo-)polymerization (CROP) and have been studied extensively[16]. Significant advancements have been made in the free-radical polymerization (FRP) of acrylates, where the $[(Cp)Fe(arene)]^+$ complexes are also employed, either as mono-component radical initiators—as demonstrated for **Fc-NBP**[17]—or as part of multicomponent systems. In the latter case, photoinitiators such as tris (2-((4-nitrophenyl)-iminomethyl)pyridine)iron(II) ($Fe^{II}(NO_2$**-PIMP**$)_3$) are combined with

J. Tolboom, J. Bootsma, B. de Bruin
Homogeneous, Supramolecular and Bio-Inspired Catalysis Group
Van 't Hoff Institute for Molecular Sciences
University of Amsterdam
Science Park 904, 1098 XH Amsterdam, Netherlands
E-mail: b.debruin@uva.nl

A. K. Bauer
Department of Chemistry
University of Rochester
Rochester, New York 14627, USA

A. K. Bauer, M. L. Neidig
Department of Chemistry
Inorganic Chemistry Laboratory
University of Oxford
Oxford OX13QR, UK

J. Flapper
Akzo Nobel Decorative Coatings B.V.
Rijksstraatweg 31, 2171 AJ Sassenheim, Netherlands

Supporting information for this article is available on the WWW under https://doi.org/10.1002/ceur.202500104

Research Article
doi.org/10.1002/ceur.202500104

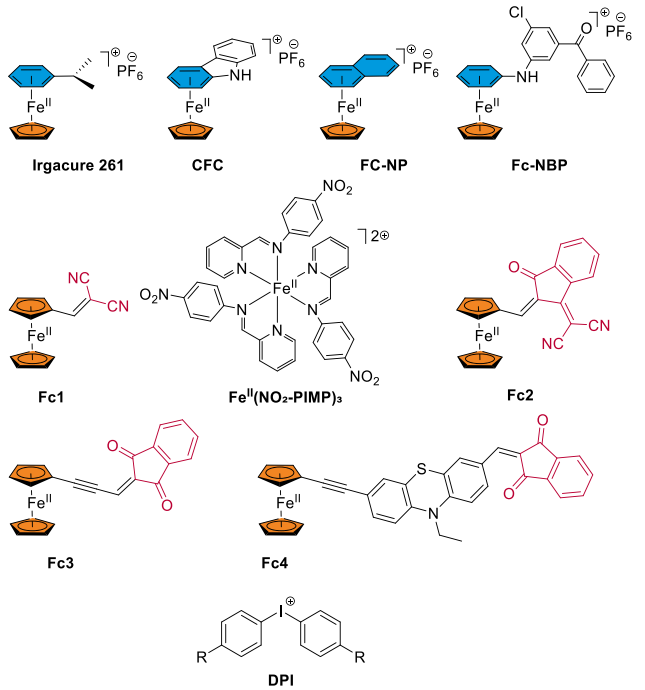

Scheme 1. Iron-based photoinitiators for cationic photopolymerization and ferrocene- or pyridine (imine)-based iron photocatalysts used in multicomponent FRP of acrylates when combined with **DPI**.

additives like diphenyliodonium salts (DPI), which generate radicals upon photoactivation.[18–24] Ferrocene-based push–pull photoinitiators, including **Fc1**, **Fc2**, **Fc3**, and **Fc4**, are attracting increasing attention for FRP due to their ability to be activated by near-infrared light.[25–26]

In this study, we investigate the drying of alkyd paints: polyester oligomers bearing bio-based unsaturated fatty-acid side chains that undergo oxidative crosslinking (**Scheme 2**). This crosslinking process differs from CROP and FRP, as it proceeds via hydrogen atom transfer (HAT) at bis-allylic sites of unsaturated fatty acid side chains. The resulting carbon-centered radicals subsequently react with molecular oxygen, leading to oxygen-driven crosslink formation and ultimately a dry paint film. The natural drying process typically takes a long time and is catalyzed by a redox-active, transition metal catalyst (Scheme 2a).[27–28] Previous iron-based catalysts for alkyd drying include Fe^{II} salts combined with polypyridyl ligands (Scheme 2b).[29] One example of these ligands is **bispidon**[30]. Further ligand systems with good curing performance are **MeN$_4$py**, **L1** and **L2** (Scheme 2b). These ligands are pentadentate ligands known to generate very active catalysts for alkyd resin curing when coordinated to Fe^{II}.

In this paper we focus on optimizing previously reported additive-free light-activated Fe-catalysts used as latent alkyd paint curing agents to replace traditional cobalt soaps (**Scheme 3**a)[31]. The key idea is that the catalyst should become active only when applied on a surface exposed to ambient air and light (Scheme 3b), introducing latency and eliminating the use of anti-skinning agents such as 2-butanone oxime (MEKO) or other oximes[32–33]. Both cobalt and oximes are currently under legislative pressure, and the development of new latent Fe-based catalyst

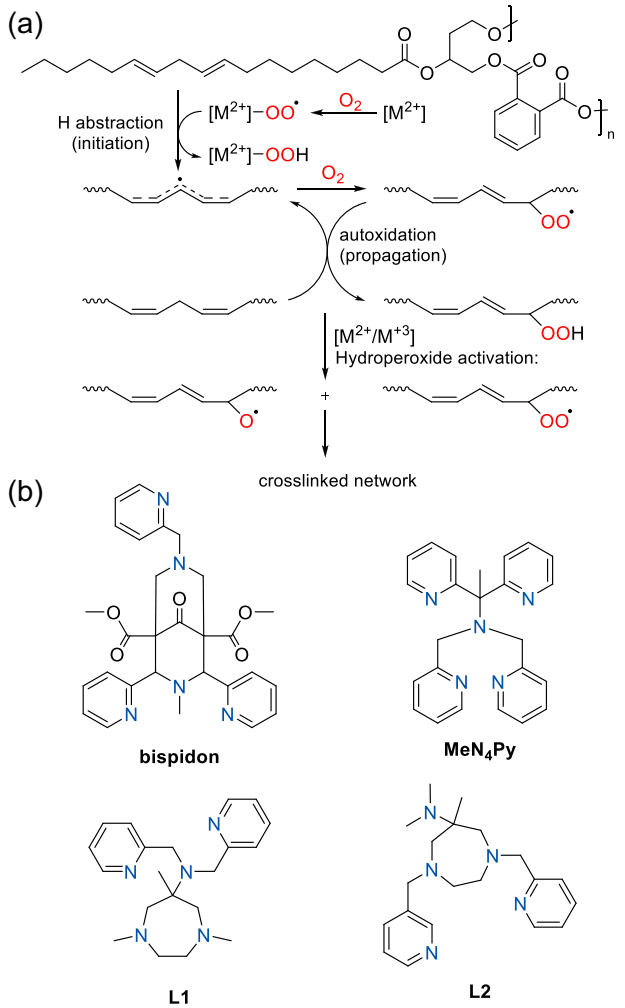

Scheme 2. a) Mechanism of alkyd curing (cross-linking) using metal-based catalysts.[27–28] b) Ligands exhibiting paint drying activity when mixed with Fe^{II} salts or as preformed Fe^{II}-ligand complexes.[29–30]

for alkyd-paint may thus contribute to more sustainable alkyd-paint formulations.[27,30–36] Recently our group showed that [(η^5-cyclopentadienyl)-(η^6-benzene)iron(II)]$^+$ (**1**$^+$) and its methylated counterpart [(η^5-cyclopentadienyl)(η^6-toluene) iron(II)]$^+$ (**1**$'^+$) can be used as efficient visible-light-triggered catalysts for alkyd resin crosslinking.[31] Upon photoactivation and during the drying process, the initial light yellow color of these complexes disappears.

In addition, [(Cp)Fe^{II}(benzene)](PF$_6$) (**1**)-derived complexes are thermally stable and remain inactive in the dark—ensuring long-term shelf stability—even after extended storage.[14,15,31] These characteristics make them attractive candidates for controlled, on-demand alkyd paint drying. However, there are still some challenges associated with the direct application of these photo-activated Fe-complexes: (1) Upon photoactivation, [(Cp)Fe(benzene)]$^+$ derived complexes release small amounts of volatile organic compounds (VOCs) such as benzene and toluene that are harmful[37]. (2) While toluene is relatively nontoxic compared to benzene, the photodissociation of [(Cp)Fe^{II}(toluene)] (PF$_6$) (**1**$'$) has a lower quantum yield (0.62 in CH_2Cl_2) than **1** (0.75 in CH_2Cl_2).[38–39]

Research Article
doi.org/10.1002/ceur.202500104

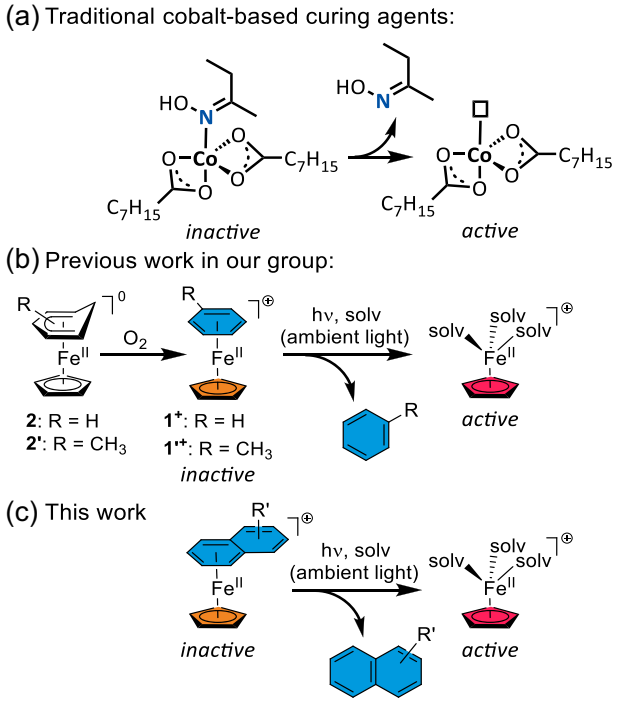

Scheme 3. a) Traditional cobalt-based curing agents require MEKO as an anti-skinning agent to achieve latency. b) Aerobic oxidation of [(Cp)Fe^{II}(Ch)] (R = H) (**2**) or [(Cp)Fe^{II}(Ch′)] (R = CH_3) (**2′**) results in the *in situ* formation of the corresponding light-sensitive [(Cp)Fe^{II}(arene)]$^+$ complexes **1**$^+$ and **1′**$^+$. These complexes, upon photoactivation, generate active Fe^{II} catalysts for alkyd paint curing (solv = solvents or ligated groups of the alkyd binder).[31] c) [(Cp)Fe^{II}(naphthalene)]$^+$ (**3**$^+$) derivatives enhance visible-light absorption and photosensitivity for curing pigmented alkyd paints.

The increase in the steric hindrance of such systems lowers the possibility of arene dissociation.[38–40] This shows that the safer iron-arene photo-initiator has lower photosensitivity.

(3) Most importantly, the [(Cp)Fe^{II}(benzene)]$^+$ derived complexes exhibit low extinction coefficients and corresponding photosensitivity,[14] which may limit their effectiveness in paints that contain dark-colored pigments capable of absorbing light across the entire spectrum (**Scheme 4**).[41–45] This presents a significant challenge for the application of light-activated catalysts in paint, as such pigments hinder light penetration and scattering, both of which are essential for initiating the photochemical activation of catalysts and triggering the crosslinking reactions required for curing.

Here we present a solution to these specific problems by red-shifting the absorbance of the pre-catalysts, while simultaneously enhancing their extinction coefficient and photosensitivity to facilitate curing of pigmented alkyd paints (Scheme 3c). This is achieved by using [(Cp)Fe^{II}(naphthalene)](PF_6) (**3**) derivatives, which, in addition to their photophysical properties, also release naphthalenes—a class of compound less volatile than arenes—thereby reducing VOC exposure during application.

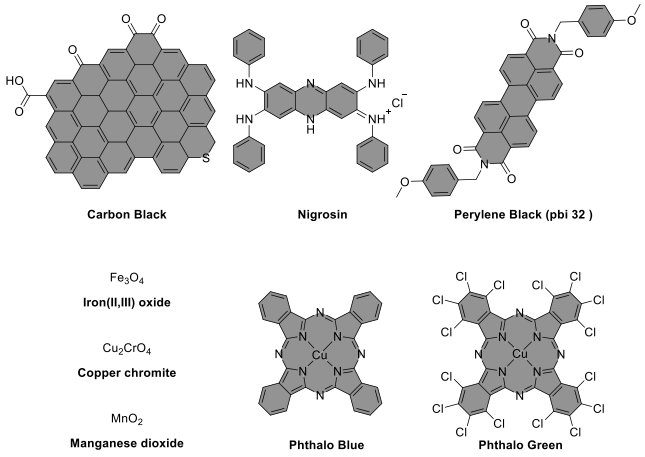

Scheme 4. Chemical structures of common dark pigments used in alkyd paints.[41–45]

2. Results and Discussion

The [(Cp)Fe^{II}(naphthalene)](PF_6) complex (**3**) is a previously reported photoactivated catalysts for epoxide polymerization, wherein it has demonstrated increased performance over **1**.[14] Motivated by these results, we explored the catalytic activity of complex **3** and a series of methoxylated derivatives—[(Cp)Fe^{II}(5-methoxynaphthalene)](PF_6) (**3-OMe**), [(Cp)Fe^{II}(6-methoxynaphthalene)] (PF_6) (**3-OMe′**), and [(Cp)Fe^{II} (5,8-dimethoxynaphthalene)](PF_6) (**3-OMe_2**)[46,47]—along with the reduced analog of the latter, **3OMe_2H** (**Scheme 5**)[48]. Their performance was evaluated in drying both transparent and pigmented alkyd paints and compared to that of complex **1**[31]. To ensure consistency across the series, and because counterions are known to significantly influence the photodecomposition behavior of these iron complexes,[49] the weakly coordinating PF_6^- anion was used as the counterion for all cationic iron complexes.

Photolabile [(Cp)Fe^{II}(arene)] (PF_6) complexes (Scheme 3b) are generally synthesized from ferrocene and $AlCl_3$ in the presence of excess arene.[50–52] However, the corresponding complexes containing naphthalene derivatives cannot be synthesized in this manner. Therefore, we moved to the synthesis of the naphthalene and pyrene derivatives using $TiCl_4$ as an additional reagent (Scheme 5). The titanium reagent traps the cyclopentadienyl ligand liberated from ferrocene (to form titanocene dichloride)[53]. This procedure was used to synthesize both **3** and [(Cp)Fe^{II}(pyrene)](PF_6) (**4**). Subsequently, **4** was used to synthesize the methoxy-derivatives of **3** by making use of the higher propensity of the pyrene ligand to undergo haptotropic ring-slippage to provide free coordination sites for the incoming arene/naphthalene (Scheme 5).[46,47,54–56]

The molar extinction coefficients markedly increase when the arene ring is substituted by a naphthalene derivative, as illustrated in **Figure 1**a and **Table 1**. A clearly enhanced absorbance is observed on going from the benzene complex to the naphthalene complex,[14] and the extinction coefficient could further be increased by introduction of methoxy substituents to the naphthalene ring. The absorbance maximum redshifted from 454 nm for **1** to 482.5 nm for **3**, and even to 489 nm for **3-OMe_2**.

Research Article
doi.org/10.1002/ceur.202500104

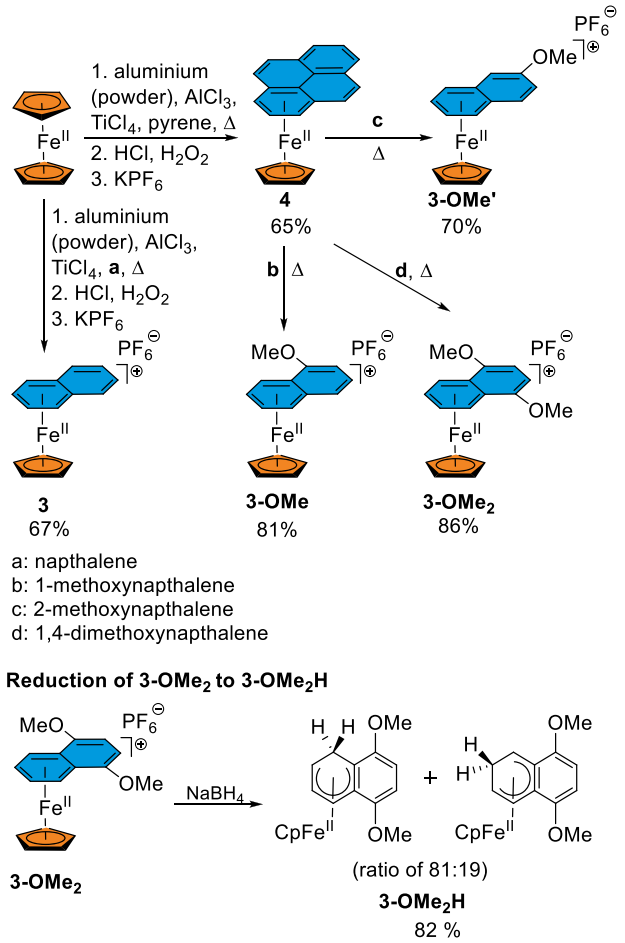

Scheme 5. Synthesis of [(Cp)Fe^{II}(naphthalene)](PF$_6$) (**3**) and its methoxylated derivatives.[46, 47]

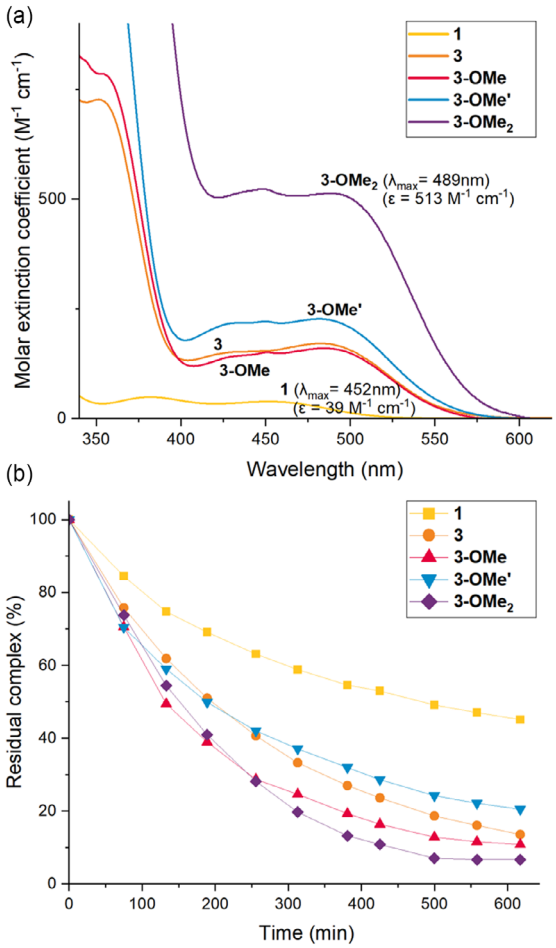

Figure 1. a) UV/Vis absorption spectra of complexes **1**, **3**, **3OMe**, **3-OMe'**, and **3-OMe$_2$** in acetonitrile. b) Relative rate of the photolysis of the different iron-complexes in acetonitriled$_3$ under 0.4 mW/m^2 light using ^{1}H-NMR (Figure S27, Supporting Information), displaying a faster photolysis of the naphthalene derivatives compared to **1**.

2.1. TD-DFT Calculations

To gain more insight into the extinction coefficients of the initial complexes, time-dependent density functional theory (TD-DFT) calculations on the optimized geometries were performed using Turbomole (op-be, def2-TZVP, m4) (Supporting Information S35-S53) to confirm the origin of the absorbance bands. The electronic transitions were calculated, including implicit solvent corrections (dielectric constant = 37.5, refractive index = 1.344). The calculated bands reproduced the experimental UV-Vis-NIR absorption spectra (Figure S34-S38, Supporting Information), confirming the suitability of the chosen computational model. Furthermore, they were in good agreement with previous DFT calculations performed on the [(Cp)Fe^{II}(arene)]$^+$ system.[56,57] Inspection of the most relevant excitations (Supporting Information S39-S52) reveal that the most intense absorbance bands shift from primarily metal-centered transitions (d_z^2-d_{xy}*/d_{yz}*)[57–59] to more ligand-involved transitions (L_π-d_{xy}*/d_{yz}*) (Figure S34-S38, Supporting Information). This trend is also observed in the methoxy-substituted derivatives, where increased electron density in the non-coordinating ring of the naphthalene further enhances intramolecular charge transfer. As a result, these complexes exhibit redshifted and more intense absorption bands.

Table 1. Absorbance maximum and corresponding extinction coefficients for [(Cp)Fe^{II}(benzene)](PF$_6$) (**1**) and the iron-naphthalene complexes **3**, **3-OMe**, **3-OMe'**, and **3-OMe2**.

	1	3	3-OMe	3-OMe'	3-OMe2
λ_{max} (nm)	452	482	484	480	489
ε (M^{1}cm^1)	39	171	160	227	513

2.2. Photolysis Rate of the Cationic Complexes and Enhanced Photoactivation of the Naphthalene Derivatives

To investigate whether the higher extinction coefficients and difference in structure of the naphthalene-based complexes **3**, **3-OMe**, **3-OMe'** and **3-OMe$_2$** result in faster photochemical catalyst activation compared to complex **1** (Table 1), we studied the kinetics of photochemical activation in acetonitrile (ACN) under irradiation (Figure 1b). Upon photolysis in acetonitrile, it is known that [(Cp)Fe^{II}(arene)]$^+$ complexes undergo arene dissociation, yielding the metastable [(Cp)Fe^{II}(ACN)$_3$]$^+$ intermediate, which subsequently disproportionates to ferrocene and Fe(II) ions.[31,58,59]

Research Article
doi.org/10.1002/ceur.202500104

To quantify the rate of photo-chemical activation, we monitored the decrease in the concentration of the iron–arene complexes by ^{1}H-NMR spectroscopy using trimethoxybenzene as an internal standard (Figure 1b). As anticipated, photo-induced arene dissociation from complexes **3**, **3-OMe**, **3-OMe'**, and **3-OMe$_2$** is significantly faster than benzene dissociation from complex **1**. After 300 min of irradiation in acetonitrile-d_3, more than 60% of the naphthalene-derived complexes had converted, with dissociation levels exceeding 75% after 600 min. In comparison, complex **1** showed substantially slower photo-reactivity under identical conditions, with only 40% and 50% conversion after 300 and 600 min, respectively. Among the naphthalene derivatives, complex **3-OMe$_2$** displayed the most rapid photo-dissociation, achieving near-complete conversion within the monitored timeframe.

Interestingly, the extinction coefficient of complex **3OMe$_2$** appears to be approximately three times higher than that of **3-OMe** (Figure 1a). However, the decomposition rate of these two complexes appears to be very similar (Figure 1b). This observation suggests that the increased steric bulk introduced by the additional methoxy substituent in **3-OMe$_2$** hinders ligand exchange via an associative mechanism. Specifically, the presence of a second methoxy group on the naphthalene ring likely introduces steric shielding around the photoexcited iron center, limiting the accessibility of incoming solvent molecules required for coordination and subsequent dissociation. As a result, despite the higher light absorption capacity of **3-OMe$_2$**, the overall rate of photodecomposition is not significantly enhanced relative to **3-OMe**, highlighting the influence of steric effects on the efficiency of photochemical activation.

Furthermore, for the complexes **3**, **3-OMe** and **3-OMe'** the relevant absorbance bands are d_z^2-d_{xy}*/d_{yz}* transitions (See TD-DFT calculations), which is the most efficient excitation for arene ring dissociation, the relevant absorbance bands of **3-OMe$_2$** are L_π-d_{xy}*/d_{yz}* transitions. The latter can still lead to arene dissociation, but less efficiently (TD-DFT Supporting Information).

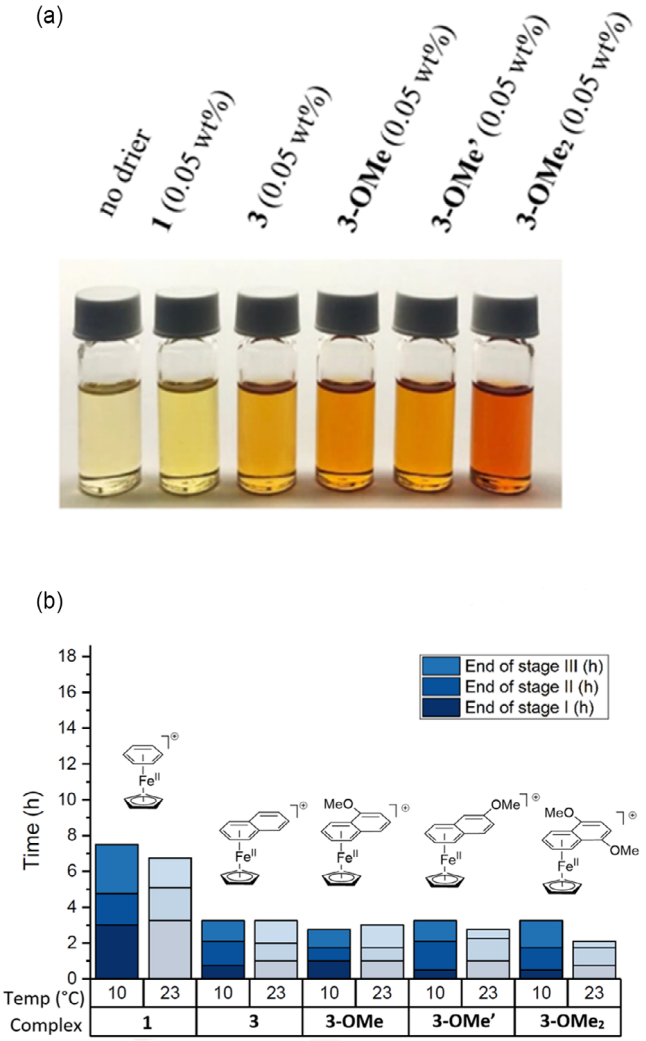

Figure 2. a) Prepared paint samples, from left to right: transparent setal-270 binder, and setal loaded with complexes **1**, **3**, **3OMe**, **3-OMe'**, and **3-OMe$_2$** (0.05 wt% metal relative to binder contents). b) Drying times of alkyd films containing complexes **1**, **3**, **3-OMe**, **3-OMe'**, and **3-OMe$_2$** under two conditions: 10 °C /85% Relative Humidity (RH) /190 Lx (2.7 mW/m^2) and 23 °C /50% RH /116 Lx (1.7 mW/m^2).

2.3. BK Drying Times and Hardness Development in Transparent Paint Samples

Subsequently, the more strongly light-absorbing naphthalene-based catalysts were evaluated as driers (0.05 wt% Fe vs. solid binder) in the soybean-based alkyd resin Setal-270 (**Figure 2**a). Initial BK drying tests (see Supporting Information for details) were conducted under two conditions—10 °C at 85% relative humidity (RH) (190 Lx /2.7 mW m^{-2}), and 23 °C at 50% RH (116 Lx / 1.7 mW m^{-2}) on 90 μm thick films (Figure S26, Supporting Information). Compared to complex **1** (≈7 h drying time), the naphthalene-based catalysts **3** and its derivatives show significantly reduced drying times (≈3 h) under ambient lighting (190 Lx / 2.7 mW m^{-2}) at the same catalyst loading (Figure 2b). This enhancement aligns with our hypothesis that the more photolabile and stronger light-absorbing naphthalene complexes should more rapidly be photoactivated, and hence cure the alkyd paints faster.

Consistent with prior observations for complex **1**, no curing was observed for alkyd films containing complex **3** and its derivatives when stored in the absence of light for more than 24 h. Notably, transparent film measurements confirm that the iron–naphthalene catalysts cure faster than complex **1** under both low (10 °C) and ambient (23 °C) temperatures. The drying times achieved are comparable to those of conventional driers containing additional secondary driers: CoNeo (0.125 wt%, 2 h), BOC (0.00125 wt%, 4.5 h), and Mn/MeTACN (0.0125 wt%, 2.5 h).[30,31] Particularly notable is the robust performance of the iron complexes at 10 °C, a condition under which cobalt-based systems such as CoNeo are known to lose efficacy, especially under high humidity.[30] This highlights a distinct advantage of the iron-based systems under more challenging curing environments.

The hardness development of coatings dried with **1**, **3**, **3-OMe**, **3-OMe'**, and **3-OMe$_2$** was evaluated using the König pendulum damping test, which quantifies coating hardness based on the damping behavior of an oscillating pendulum. All coatings were prepared using 0.05 wt% metal relative to binder content. The films

Research Article
doi.org/10.1002/ceur.202500104

cured with **1**, **3**, **3-OMe**, **3-OMe'**, and **3-OMe$_2$** exhibit comparable hardness values (**Table 2**), demonstrating consistent performance across this series. However, the commercial cobalt-based drier (0.079–0.125 wt%) is known to achieve a higher final hardness of 25–40 oscillations,[30–31] surpassing the iron systems at the concentrations tested in this study. In contrast, the commercial manganese-based catalyst Mn/MeTACN results in a lower final hardness of only 15.[31] It should be noted that the studies references above employed secondary driers, such as zirconium and calcium carboxylates.

2.4. Drying Time Efficiency, Time-Resolved Fourier Transform Infrared (FT-IR) Spectroscopy and Curing Kinetics

Time-resolved FT-IR spectroscopy was employed to monitor the curing kinetics of alkyd paints containing the iron-based catalysts under constant light irradiation (0.4 mW m^{-2}).[31] The observed spectral changes in Setal-270 alkyd resin dosed with complex **3** and its methoxy-substituted derivatives closely mirrored those previously recorded for curing with complex **1** and the commercial cobalt-based drier CoNeo (Figure S43, Supporting Information). Specifically, the disappearance of the cis-alkene signal at 3008 cm^{-1} and the emergence of a broad hydroxyl band around 3400 cm^{-1} were noted, corresponding to alkene consumption and the formation of hydroxylated species during oxidative crosslinking.[60] At 0.05 wt% Fe loading, complex **3** and its methoxy-derivatives showed substantially faster cis-alkene conversion than complex **1**, consistent with the BK recording results (**Figure3**a).

In addition to a faster rate, the **3**-derived complexes also exhibited shorter incubation times, indicating quicker initiation of the curing process. The curing profile followed a weak exponential decay in the cis-alkene concentration, in line with the rate of photoinduced ligand dissociation observed by ^{1}H-NMR (Figure 1b). These results confirm that the more photolabile naphthalene-based complexes outperform **1** in terms of curing kinetics (Figure 3a). Remarkably, despite being applied at a relatively low concentration (0.05 wt% Fe relative to binder solids), the iron–naphthalene complexes demonstrate curing performance that is still competitive with commercial driers: CoNeo (0.125 wt%), Mn/TACN (0.0125 wt%), and BOC (0.00125 wt%) (Figure 3b).[31]

2.5. Light-Induced Latency and Curing Rate

To investigate the light-dependency of the catalytic activity, 90 μm thin films of Setal-270, containing 0.05 wt% of the photoactivatable iron-driers were prepared. These films were kept in the dark and intermittently exposed to low intensity light (0.4 mW/m^2) for 30 min intervals. During the periods of illumination, a notably increased conversion was observed via FT-IR (**Figure 4**a), indicating that the catalytically active species is formed only upon irradiation. As such, constant exposure to light is required to obtain a fully hard and cured coating in a short time.

When the light was turned off, the conversion continues at a lower rate and further slows down over time. This observation suggests that, once the active Fe species is formed, it can initiate the autoxidation process, which then proceeds for a while in the absence of further light exposure. This behavior is consistent with the mechanism proposed in Scheme 2a.

To determine whether a short time of ambient light exposure, and consequently a limited amount of activated Fe would be sufficient to drive full curing, the most active complex for curing transparent paint (complex **3OMe**) was selected for further studies. Setal-270 films (90 μm thick) containing 0.05 wt% of

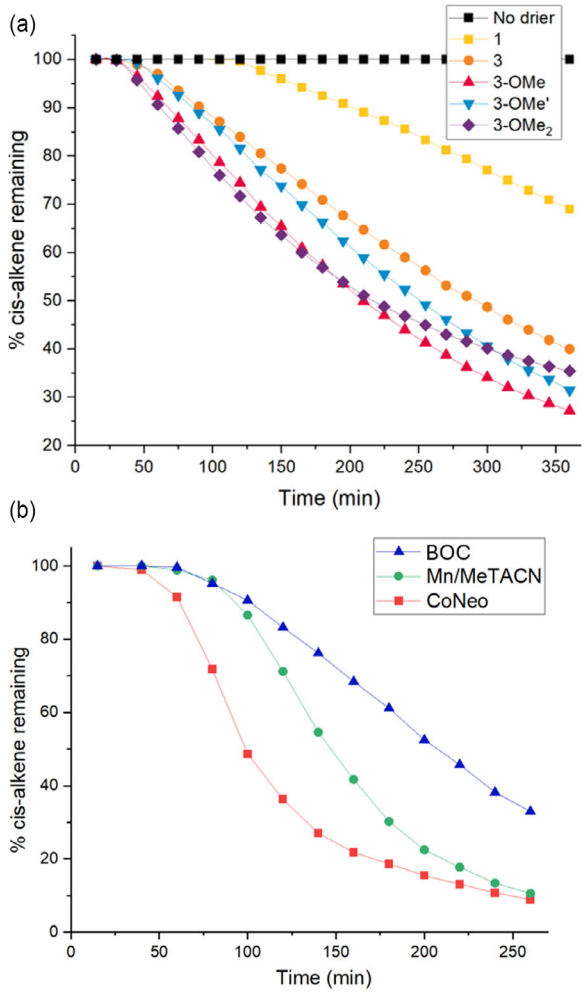

Figure 3. a) Conversion of cis-alkene in Setal-270 using FT-IR for the iron catalysts **1**, **3**, and the methoxy derivatives of **3** (all used at 0.05 wt% Fe) under 0.4 mW/m^2 light, monitored by the decrease in absorbance at 3008 cm^{-1}. The black line shows the decrease in absorbance at 3008 cm^{-1} without added catalyst. b) Conversion of cis-alkene (3008 cm^{-1}) in Setal-270 for CoNeo (0.125 wt%), Mn/TACN (0.0125 wt%), and iron bispidon as Borchi OXY-Coat (BOC) (0.00125 wt%).

Table 2. Hardness values (number of oscillations, average of duplicate) for 90 μm transparent paint films, using the König pendulum test.

Time[a)]	1	3	3-OMe	3-OMe'	3-OMe$_2$
1 day	9	12	11	10	12
2 days	16	17	14	14	15
3 days	18	20	17	16	16
7 days	20	23	18	17	18
14 days	22	23	21	19	20

[a)]The samples were stored at 23 °C and 50% relative humidity.

Research Article
doi.org/10.1002/ceur.202500104

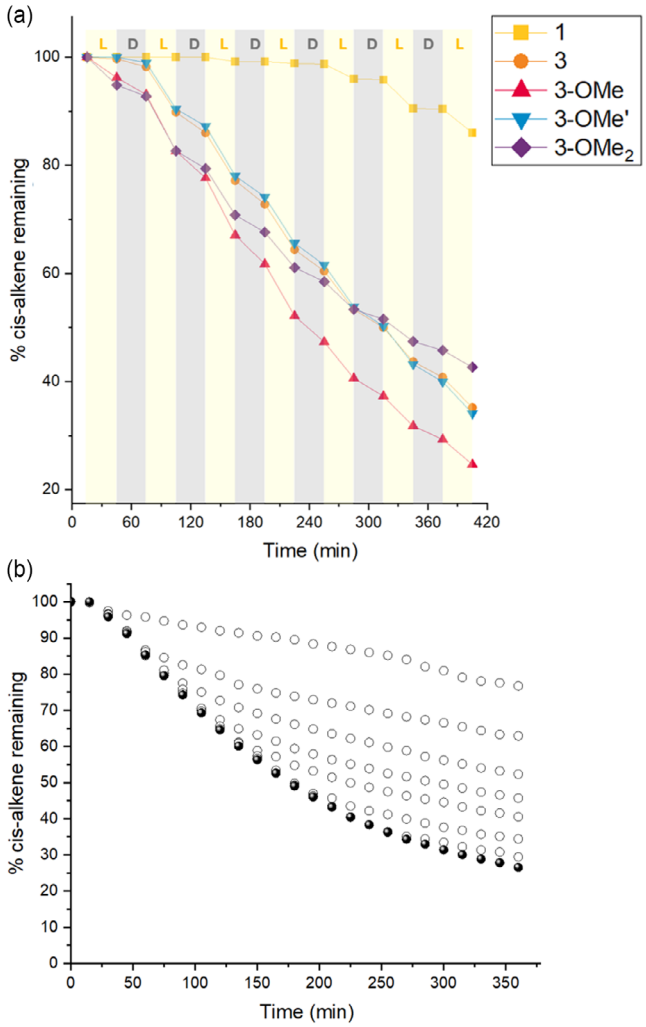

Figure 4. a) FT-IR-monitored cis-alkene conversion under alternating 30-minute intervals of darkness (D) and light (L, 0.4 mW/m^2) for samples with 0.05 wt% drier shows a strong correlation between light exposure and conversion. b) Cis-alkene conversion for sample **3-OMe** under irradiation with lightbox setup (light 0.4 mW/m^2; closed circles) and samples moved to a dark area (open circles).[31]

3OMe were first irradiated with 0.4 mW m^{-2} light and subsequently transferred to dark conditions to monitor the curing process over time (Figure 4b). This procedure was repeated after light exposure of 15, 60, 75, 105, 135, and 195 min. For all samples transferred to the dark, curing continued for some time but gradually diminished and eventually plateaued, indicating that no further drying occurred once the active Fe species were depleted. The decline in conversion rate observed in both Figure 4a and b is attributed to the rapid transformation of the active Fe species into catalytically inactive forms. The minimal discoloration observed after curing suggests that these inactive species are likely Fe^{III} oxides or oxyhydroxides, in agreement with previous reports[31,61,62].

2.6. Mössbauer Spectroscopic Data

To gain deeper insight into the nature of the iron species formed within the alkyd paint matrix under aerobic conditions, ^{57}Fe Mössbauer spectroscopy was employed at 80 K. This technique allows to determine the iron oxidation states and coordination environments after light activation and curing. For this purpose, both ^{57}Fe-labelled versions of complex **1** and complex **3** were synthesized (Supporting Information S18-S19). Two Setal 270 alkyd paint formulations were prepared, each containing 0.05 wt% of the corresponding ^{57}Fe–labelled complex **1** or complex **3**.

After formulation, the paints were stored in a closed dark vial for 24 h to ensure homogeneity. They were then applied to a glass plate (30 cm in length) using a 90 μm applicator, under conditions identical to those used for the BK measurements. The coated samples were left to dry under ambient conditions and presence of light (250 Lux/3.6 mW m^{-2}). Mössbauer spectra were collected from one half of each sample after 1 h of drying; the other half was analyzed after 2 h.

Analysis of the samples containing [(Cp)^{57}Fe^{II}(benzene)](PF$_6$) (**1**) revealed two distinct species (**Figure 5**a, blue and orange lines). The major species (74%, blue line) with isomer shift $\delta = 0.52$ mm s^{-1} and quadrupole splitting parameters $|\Delta E_Q| = 1.67$ mm s^{-1} corresponds to the starting complex, i.e. the cationic low-spin [(Cp)Fe^{II}(benzene)]$^+$ species (Figure S17, Supporting Information)[57,63]. After two hours, only 57% of this species was left, while the signal of a high-spin Fe^{III} species (orange line; $\delta = 0.51$ mm s^{-1}, $|\Delta E_Q| = 0.67$ mm s^{-1}) had increased from 26% (after 1 h) to 43% (after 2 h). This signal most likely stems from deactivated high-spin Fe^{III} species that are no longer catalytically active, as suggested by the light-induced latency kinetics.

Under the same conditions, the sample containing [(Cp)^{57}Fe^{II}(naphthalene)](PF$_6$) (**3**) also showed the presence of two major species (Figure 5b). The starting cationic low-spin [(Cp)Fe^{II}(naphthalene)]$^+$ complex (green line) was present in 53% after 1 h ($\delta = 0.55$ mm s^{-1} and $\Delta E_Q = 1.79$ mm s^{-1}). Deactivated high-spin Fe^{III} species was also observed (yellow line; 42%, $\delta = 0.52$ mm s^{-1}, $\Delta E_Q = 0.56$ mm s^{-1}). After 2 h, 40% of the the low spin [(Cp)Fe^{II}(naphthalene)]$^+$ complex was left, and the amount of deactivated high-spin Fe^{III} species had increased to 60%.

Interestingly, during curing of paint with complex **3** a minor, third species (pink line, 5%) was also detected after 1hr ($\delta = 1.37$ mm s^{-1}, $|\Delta E_Q| = 2.68$ mm s^{-1}, 5%), consistent with a high-spin Fe^{II} species. This high-spin iron(II) species is most likely a [(Cp)Fe^{II}(solv)]$^+$ species (Scheme 3b), where solv represents solvent or a donating group of the alkyd binder. This species is likely formed directly upon photo-induced dissociation of naphthalene from the [(Cp)Fe^{II}(naphthalene)]$^+$ complex. This high-spin Fe^{II} (pink line, Figure 5b) species is proposed to be a reactive intermediate towards O_2 and/or peroxides present in the alkyd binder. As such, we anticipated higher concentrations of this species upon photo-activation of [(Cp)Fe^{II}(naphthalene)] (PF$_6$) under anaerobic conditions using a peroxide-free alkyd binder. This is indeed the case. An O_2 and peroxide-free binder was prepared by filtering the alkyd resin over neutral alumina using acetone as a solvent, after which the solvent was evaporated. Subsequently the alkyd was subjected to freeze-pump-thaw cycles to remove residual O_2. All subsequent steps were performed inside a nitrogen-filled glovebox. The paint formulation was prepared using dry and degassed solvent and kept in a dark vial for 24. After this period, the samples were transferred into transparent vials and

Research Article
doi.org/10.1002/ceur.202500104

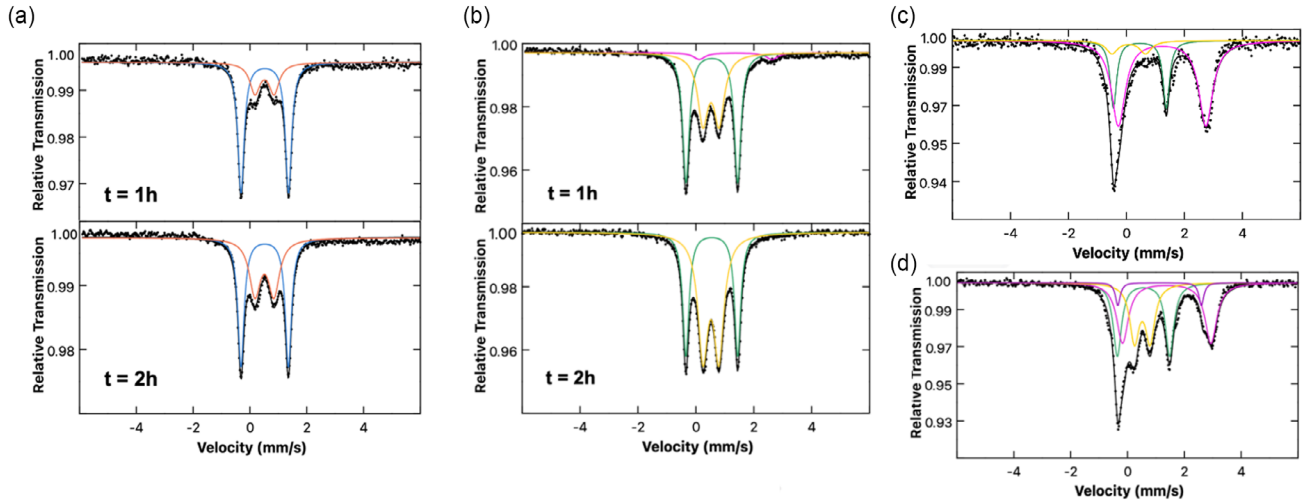

Figure 5. a) Aerobic freeze-trapped 80 K ^{57}Fe Mössbauer spectra of light-activated [(Cp)^{57}Fe^{II}(benzene)](PF$_6$) (**1**) (blue; $\delta = 0.52$ mm s^{-1}, $|\Delta E_Q| = 1.67$ mm s^{-1}) reacting with Setal-270 alkyd resin after 1 h, showing 26% formation of a deactivated Fe^{III} species (orange; $\delta = 0.51$ mm s^{-1}, $|\Delta E_Q| = 0.67$ mm s^{-1}), increasing to 43% after 2 h. b) Same experiment with [(Cp)^{57}Fe^{II} (naphthalene)](PF$_6$) (**3**) (green; $\delta = 0.55$ mm s^{-1}, $|\Delta E_Q| = 1.79$ mm s^{-1}), yielding 42% Fe^{III} species (yellow; $\delta = 0.52$ mm s^{-1}, $|\Delta E_Q| = 0.56$ mm s^{-1}) after 1 h, increasing to 60% after 2 h. c) Anaerobic conditions: light-activated [(Cp)Fe^{II}(naphthalene)](PF$_6$) (green, 25%) in Setal-270 after 2 h forms a 69% high-spin Fe^{II} species (pink; $\delta = 1.37$ mm s^{-1}, $|\Delta E_Q| = 2.68$ mm s^{-1}), and a minor (9%) Fe^{III} species (yellow; $\delta = 0.52$ mm s^{-1}, $|\Delta E_Q| = 0.56$ mm s^{-1}) is present. d) After 2 h anaerobic light-activation followed by exposure to aerobic conditions, [(Cp)^{57}Fe^{II}(naphthalene)](PF$_6$) (green, 31%) in Setal-270 forms a high-spin Fe^{II} species (pink, 36%), a high-spin Fe^{III} species (yellow, 27%), and a second high-spin Fe^{II} species (purple, 6%; $\delta = 1.10$ mm s^{-1}, $|\Delta E_Q| = 2.84$ mm s^{-1}).

subjected to controlled photoactivation using a slightly higher light-intensity (290 Lx /4.143 mW m^{-2}) compared to the aerobic samples. After 10 min of illumination, the samples remained liquid, indicating that no oxidative curing had occurred due to absence of O_2. One of the samples was transferred to a Mössbauer sample cup for analysis. As expected, this sample contained a substantial higher concentration of the abovementioned high-spin iron(II) [(Cp)Fe^{II}(solv)]$^+$ species, reaching 33% already after 10 min of irradiation (Figure S19, Supporting Information, pink). This is in agreement with the relatively fast photo-activation of [(Cp)Fe^{II}(naphthalene)]$^+$ shown in Figure 1.

After 2 h of continued photoactivation (Figure 5c) the samples were still liquid, further confirming that oxygen is essential for initiating the oxidative cross-linking reactions required for film formation. The contents of the vials were then transferred to two Mössbauer sample cups. One of the samples was frozen under liquid nitrogen prior to measurement (Figure 5c). The resulting Mössbauer spectrum revealed formation of the high-spin [(Cp)Fe^{II}(solv)]$^+$ species in 69% yield. These results support that, in the absence of O_2, the photogenerated high-spin Fe^{II} intermediate (pink line) remains stable and does not convert into other species, leading to build-up of the high-spin [(Cp)Fe^{II}(solv)]$^+$ (Supporting information S19-S23).

To investigate the effect of reintroducing oxygen, the second sample—photoactivated for 2 h under anaerobic conditions—was removed from the glovebox and exposed to air for 5 min prior to Freeze-trapped 80 K ^{57}Fe Mössbauer analysis.

The resulting spectrum (Figure 5d) showed that 31% of the [(Cp)Fe^{II}(naphthalene)]$^+$ species was present, comparable to the amount observed in the fully anaerobic sample (Figure 5c). The high-spin [(Cp)Fe^{II}(solv)]$^+$ species was still present but had decreased significantly to 36%, down from 69% in the nitrogen-protected sample. Upon exposure to air, a substantial part of the high-spin [(Cp)Fe^{II}(solv)]$^+$ (pink line, Figure 5c) species converted to the abovementioned deactivated high-spin Fe^{III} species (27%, yellow line), consistent with prior observations. Notably, a new Fe^{II} species (6% purple line, Figure 5d) species was detected ($\delta = 1.10$ mm s^{-1}, $|\Delta E_Q| = 2.84$ mm s^{-1}), which had not been observed in the paint matrix before. This species, which appears only after exposure to air, likely results from degradation of the original complex and is tentatively assigned to a cyclopentadienyl-free Fe^{II} species. Its Mössbauer parameters resemble those reported for ferrous (Fe^{II}) oxalate (Fe^{II}(C_2O_4) · 2H_2O), suggesting a weak-field, high-spin Fe^{II} coordination environment. This may arise from Fe^{II} binding to carbonyl functionalities present in the alkyd resin[64–66].

The deactivated high-spin Fe^{III} species observed after prolonged exposure to light and air (Figure 5a, orange line; Figure 5b, yellow line) exhibit Mössbauer parameters resembling those of Fe^{III} (acac)$_3$ and ferric oxalate complexes such as Fe$^{III}_2$(C_2O_4)$_3$(H_2O)$_x$[67–69]. This similarity supports a mechanistic pathway in which the photogenerated high-spin Fe^{II} species undergoes Cp-ring dissociation followed by oxidation. These results show that the catalyst is gradually photo-converted leading to low steady state concentrations of the active high-spin Fe^{II} species. Under aerobic conditions, this species is rapidly oxidized—likely by peroxides or oxygen—into Fe^{III} species of lower activity. This supports a photoactivated curing mechanism, continuously generating enough active Fe^{II} to sustain the cross-linking process.

2.7. Application of Photolabile Iron Naphthalene Complexes in Pigmented Alkyd Paints

As mentioned above, the combination of higher extinction coefficients, a red-shifted UV–vis adsorption band and overall

Research Article
doi.org/10.1002/ceur.202500104

faster paint curing performance positions the iron–naphthalene complexes as promising candidates for application in colored alkyd paints. To explore this potential, three commercial pigment pastes were explored (**Figure 6** a,b). The blue and black pigment pastes contain phthalo blue and carbon black, respectively (Scheme 4), while the full compositions are detailed in the Supporting Information (Table S2, Supporting Information). Paint formulations were prepared using a pigment-to-binder ratio of 1:10 to assess how the pigments influence curing behavior. Optical characterization revealed that the orange and blue pigments allow partial light transmission through the film: the orange pigment absorbs light primarily around 320 nm and above 600 nm, while the blue pigment absorbs light below 350 nm and between 500 nm and 700 nm. In contrast, the black pigment absorbs broadly across the UV–Vis range (270–900 nm), effectively blocking light penetration.

2.8. Contrast-Ratio and ΔE_{2000} Analysis

To quantify the hiding power of the different pigments, a combination of UV-Vis spectroscopy (Figure S25 , Supporting Information), the contrast-ratio method, and ΔE_{2000} color difference analysis (Supporting Information S27) was employed. The contrast ratio is defined as the ratio of a material's apparent reflectance on a black background to that on a white background. Formulations were prepared using pigment-to-binder ratios of 1:10 and 1:5 (see **Table 3**) and dried with the CoNeo catalyst. As shown in Table 3, both orange and blue paint exhibited low opacity values and high ΔE_{2000} values, reflecting their limited absorption across the full light spectrum. These pigments are often combined with others in commercial formulations to enhance hiding power. The black pigment, in particular, absorbs light effectively. This observation aligns with the contrast ratio and ΔE_{2000} values in Table 3. At a pigment-to-binder ratio of 1:5, complete hiding was achieved (opacity = 100%) with a ΔE_{2000} value of just 0.06, confirming the formulation's excellent visual coverage.

Table 3. Contrast-ratio and ΔE2000 analysis for pigmented paints with a 1:10 or 1:5 pigment-to-binder ratio.

Pigment	Ratio (Pigment paste/binder)	Opacity	ΔE_{2000}
Orange (sO1)	1:10	60.1	14.0
Orange (sO1)	1:5	58.5	14.6
Blue (sB1)	1:10	27.8	25.9
Blue (sB1)	1:5	25.2	27.1
Black (sZ1)	1:10	91.4	0.6
Black (sZ1)	1:5	100.0	0.1

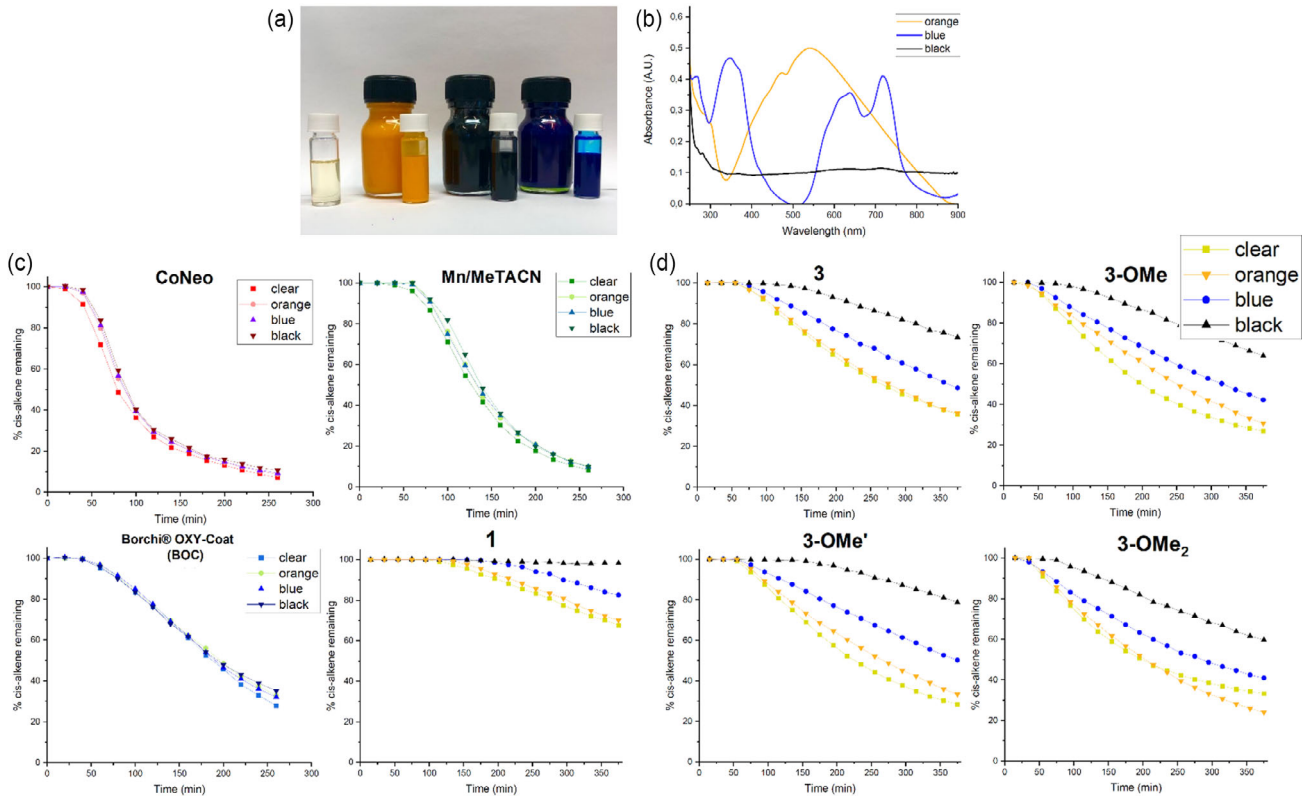

Figure 6. a) On the left, an alkyd paint without pigment is shown. The larger vials contain pigment paste, the smaller vials display pigmented alkyd paints, mixed at a 1:10 ratio of pigment to solid binder. b) UV-Vis spectrum of the pigment pastes in heptane. c) Conversion of cis-alkene monitored by FT-IR in Setal-270 formulations containing different pigments (pigment-to-alkyd ratio = 1:10) for CoNeo (0.125 wt%), Mn/TACN (0.0125 wt%), BOC (0.00125wt%) and [(Cp)Fe^{II}(benzene)](PF_6) (**1**) (0.05 wt%). d) Conversion of cis-alkene monitored by FT-IR in Setal-270 formulations containing different pigments (pigment-to-solid alkyd ratio = 1:10) incorporating **3** and its methoxylated derivatives as driers (0.05 wt%).

Research Article
doi.org/10.1002/ceur.202500104

2.9. The Influence of Pigments on the Alkyd Paint Curing Kinetics of [(Cp)Fe^{II}(benzene)](PF$_6$) Compared to Commercial Co-Neo, Mn/MeTACN and BOC Driers

To assess the impact of pigmentation on curing performance, the drying kinetics of **1** was evaluated and compared to those of commercial driers—CoNeo, Mn/MeTACN, and BOC—using transmission FT-IR spectroscopy. Monitoring the integration of the cis-alkene band (3030–2992 cm^{-1}) remained feasible even in the presence of pigment paste, allowing us to study curing rates at a pigment-to-solid alkyd ratio of 1:10 (Figure S44−46, Supporting Information). As shown in Figure 6c, the curing behavior of the commercial driers was largely unaffected by the pigments, which is expected since initiation of alkyd drying solely depends on the presence of oxygen and evaporation of MEKO in these cases. In contrast, the curing performance of the photo–latent complex **1** was clearly affected by the presence of pigments. In the presence of the orange pigment, the curing rate was comparable to that of the transparent sample, indicating that the partial light transmission of this pigment did not significantly interfere with photoactivation. However, for the blue samples, a delayed onset of paint curing was observed, accompanied by a much slower curing rate. Most notably, in the presence of black pigment, no measurable curing occurred within the 6-hour observation period. This was further confirmed by BK recorder measurements, where no drying was observed over a 12 h timeframe for the black pigmented formulation containing complex **1**.

It is worth noting that white pigments did not interfere with the curing process. On the contrary, their light-scattering properties appear to enhance catalyst activation by improving light distribution and promoting photodissociation.

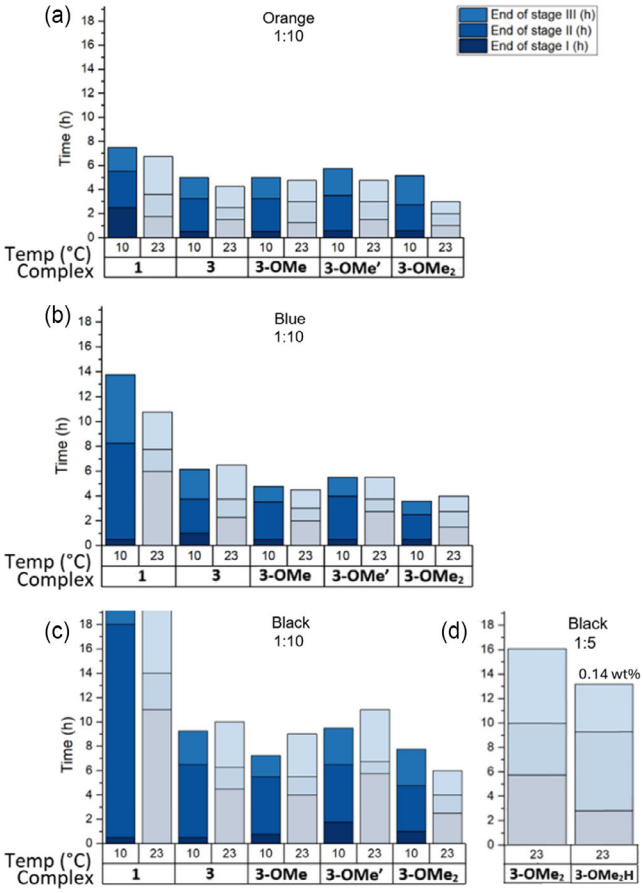

Figure 7. Paint curing in different climate rooms (10 for the room at 10 °C and light intensity of 190 Lux/2.7 mW/m^2, and 23 for the room at 23 °C and light intensity of 116 Lux/1.7 mW/m^2) for the different catalysts in alkyd paints containing different pigments in a 1:10 pigment-to-solid alkyd binder ratio. a) Orange; b) Blue; c) Black pigment.

2.10. The Influence of Pigments on the Alkyd Paint Curing Kinetics of [(Cp)Fe^{II} (naphthalene)](PF$_6$) Driers

We next investigated the effect of pigments on the curing behavior of complex **3** and its methoxylated derivatives (Figure 6d). Remarkably, these catalysts exhibited a much-reduced sensitivity to pigment interference, especially in the presence of the blue pigment paste. Most significantly, the methoxylated derivatives retained effective drying performance even in black-pigmented paints, achieving full curing within acceptable timeframes. In particular, the performance of **3-OMe$_2$** in black paints stands out, showing significantly improved curing rates relative to the parent compound and previously reported analogues.

Consistent with the FT-IR curing profiles of pigmented coatings containing **3** and its methoxylated derivatives, BK drying measurements further confirmed that the presence of orange pigment (at a 1:10 ratio) had negligible influence on the drying kinetics compared to the unpigmented (transparent) formulations (Figure 2b, **Figure 7**a). Curing delays became more pronounced upon addition of darker pigments such as the blue (Figure 7b) and black pigment pastes (Figure 7c), in which the initiation and progression of curing were slowed. Nevertheless, even under these more demanding conditions, coatings containing the naphthalene-based catalysts—especially the methoxy-functionalized versions—still achieved complete drying within 6 h, a marked improvement over complex **1**, which failed to dry under similar conditions.

Moreover, under full-hiding conditions (1:5 pigment-to-binder ratio) using black pigment paste and standard illumination (23 °C, 116 Lux/1.7 mW/m^2), **3-OMe$_2$** continued to cure the alkyd paint, albeit at a slower rate (Figure 7d). This result highlights the potential of these photo-latent catalysts to approach the performance of conventional cobalt-based driers in pigmented paint systems, although a higher concentration of the Fe catalysts might be needed to get a decent curing within an acceptable time frame. However, the cationic nature of the **3-OMe$_2$** complex limits its maximum solubility in the (apolar) alkyd matrix. Therefore, to assess our hypothesis, we chose to employ the more soluble neutral complex **3-OMe$_2$H**, which can be synthesized by $NaBH_4$ reduction of **3-OMe$_2$** (Scheme 5, Figure S16 and S33 , Supporting Information). When formulated at a higher concentration (0.14 wt% Fe) and applied in a 1:5 black pigment paste-to-binder formulation, the reduced catalyst **3-OMe$_2$H** indeed enabled faster curing, with BK-recordings indicating completion of phase 3 after 13 h (Figure 7d).

Research Article
doi.org/10.1002/ceur.202500104

2.11. Influence of Pigment Pastes on the Hardness of the Paints

König hardness measurements performed on the orange pigmented samples (1:10 pigment-paste to alkyd ratio; Supporting Information, Table S4), formulated at an iron loading of 0.05wt% vs solid binder show a similar hardness development for the different catalysts. After 14 days of drying at 23 °C, followed by post-curing at 50 °C for 100 h, the cured coatings exhibited hardness values of 30 oscillations or more (Table S4, Supporting Information).

In contrast, samples formulated with blue or black pigment generally resulted in softer films compared to transparent samples or those formulated with orange pigment (Table S5 and S6, Supporting Information), with hardness values ranging between 20 and 25 oscillations even after the same 14-day drying period and post-curing at 50 °C. This may be attributed to slower overall curing in these darker pigmented systems, and possibly to more pronounced top-down curing caused by light absorption hindering crosslinking in the lower layers of the paint film (thus leading to reduced overall hardness).

Interestingly, when examining the König hardness of catalyst **1** in the black-pigmented paint after 14 days of drying without subsequent heating, a value of 15 oscillations was observed. In contrast, all iron–naphthalene complexes already showed very acceptable König hardness values of 20 oscillations or higher at this stage, even prior to thermal post-curing.

3. Conclusion

This study demonstrates the efficacy of [(Cp)Fe^{II}(naphthalene)](PF_6) complexes as photo-latent catalysts for alkyd coating curing. These naphthalene-based systems outperform the previously reported [(Cp)Fe^{II}(benzene)](PF_6) complex, showing superior activity at lower concentrations, faster drying rates, and significantly improved performance in dark-pigmented formulations. As such, they present a broadly applicable alternative for alkyd systems, offering optimal drying and hardness without requiring anti-skinning agents.

Their activation mechanism aligns with that of other [(Cp)Fe^{II}(arene)]$^+$ complexes, reinforcing their potential as viable cobalt replacements. NMR spectroscopy confirms that the naphthalene derivatives are more photolabile than the benzene analogue, while in situ ^{57}Fe-labelled Mössbauer spectroscopy of alkyd films during the curing process reveals faster conversion of the naphthalene complex to catalytically active high-spin Fe^{II} species. Two distinct high-spin Fe^{II} species are observed—one likely corresponding to the anticipated photochemically formed [(Cp)Fe^{II}(solv)]$^+$ species, and the other appearing only in the presence of air, possibly resulting from Cp-ring dissociation.

Our investigations into pigmented systems show that white and orange pigments have only a marginal impact on the drying times of the photoactivatable iron complexes, whereas blue and black pigments significantly increase the drying times in general. Nevertheless, the [(Cp)Fe^{II}(naphthalene)](PF_6)-based catalysts show markedly reduced drying times under these challenging conditions compared to [(Cp)Fe^{II}(benzene)](PF_6), even enabling curing of black-pigmented paints within a reasonable time frame.

While these findings mark significant progress, further work is needed to enhance both curing rates and final hardness in pigmented systems to bring their performance even closer to that of commercial driers. Strategies to enhance the lifetime and/or improve the catalytic activity of the formed iron species after photoactivation are currently under investigation in our laboratory.

Acknowledgments

This work is part of the Advanced Research Center for Chemical Building Blocks, ARC CBBC (project 2022.039.A.UvA), which is cofounded and cofinanced by the Netherlands Organization for Scientific Research (NWO, contract 736.000.000) and the Netherlands Ministry of Economic Affairs and Climate.

Conflicts of Interest

The authors declares no conflicts of interest

Data Availability Statement

The data that support the findings of this study are available in the supplementary material of this article.

Keywords: [(Cp)Fe(naph]$^+$ · alkyd curing · latency · photoactive complexes · photosensitivity · pigmented paints

[1] U. Lüning, *Angew. Chem. Int. Ed* **2012**, *51*, 8163.
[2] F. A. Leibfarth, K. M. Mattson, B. P. Fors, H. A. Collins, C. J. Hawker, *Angew. Chem. Int. Ed* **2013**, *52*, 199.
[3] A. Chirila, B. G. Das, P. F. Kuijpers, V. Sinha, B. de Bruin, *In Non-Noble Metal Catalysis: Molecular Approaches and Reactions*, Vol. *1*, (Eds: R. J. Kelvin Gebbink, M. E. Moret) Wiley-VCH, Weinheim, Weinheim **2019**. pp. 1–31, ISBN: 978-3-527-69908-7.
[4] R. S. Stoll, S. Hecht, *Angew. Chem. Int. Ed* **2010**, *49*, 5054
[5] NASA Earth Observatory, *Earth's Energy Balance*, https://earthobservatory.nasa.gov/features/EnergyBalance/page2.php. (accessed May 14, 2025).
[6] Global Solar Atlas,, *Global Solar Atlas Map*, https://globalsolaratlas.info/map. (accessed May 14, 2025).
[7] H. Lai, J. Zhang, F. Xing, P. Xiao, *Chem. Soc. Rev* **2020**, *49*, 1867.
[8] N. Corrigan, J. Yeow, P. Judzewitsch, J. Xu, C. Boyer, *Angew. Chem. Int. Ed* **2019**, *58*, 5170.
[9] X. Pan, M. A. Tasdelen, J. Laun, T. Junkers, Y. Yagci, K. Matyjaszewski, *Prog. Polym. Sci* **2016**, *62*, 73.
[10] M. Chen, M. Zhong, J. A. Johnson, *Chem. Rev* **2016**, *116*, 10167.
[11] N. Corrigan, S. Shanmugam, J. Xu, C. Boyer, *Chem. Soc. Rev* **2016**, *45*, 6165.
[12] V. Andruleviciute, R. Lazauskaite, J. V. Grazulevicius, *Des. Monomers Polym* **2007**, *10*, 105.
[13] V. Andruleviciute, R. Lazauskaite, J. V. Gražulevičius, A. Stanišauskaite, *J. Photochem. Photobiol. A Chem* **2002**, *147*, 63.
[14] T. Wang, Y. L. Huang, *Imaging Sci. J* **2003**, *51*, 247.
[15] F. Lohse, H. Zweifel, *in Epoxy Resins and Composites III*, (Eds: K. D. šek), Spinger-Verlag Berlin Heidelberg GmbH Vol. *78* **1986**. pp. 61–81. Adv. Polym. Sci.
[16] F. Dumur, *Eur. Polym. J* **2020**, *139*, 110026.
[17] M. Li, Y. Chen, H. Zhang, T. Wang, *Prog. Org. Coat* **2010**, *68*, 234.
[18] J. Zhang, D. Campolo, F. Dumur, P. Xiao, J. P. Fouassier, D. Gigmes, J. Lalevée, *J. Polym. Sci. Part A Polym. Chem* **2015**, *53*, 42.

Research Article
doi.org/10.1002/ceur.202500104

[19] J. Zhang, D. Campolo, F. Dumur, P. Xiao, J. P. Fouassier, D. Gigmes, J. Lalevée, *J. Polym. Sci. Part A Polym. Chem* **2016**, *54*, 2247.
[20] J. Zhang, D. Campolo, F. Dumur, P. Xiao, J. P. Fouassier, D. Gigmes, J. Lalevée, *ChemCatChem* **2016**, *8*, 2227.
[21] S. Telitel, F. Dumur, D. Campolo, J. Poly, D. Gigmes, J. P. Fouassier, J. Lalevée, *J. Polym. Sci. Part A Polym. Chem* **2016**, *54*, 702.
[22] P. Xiao, J. Zhang, D. Campolo, F. Dumur, D. Gigmes, J. P. Fouassier, J. Lalevée, *J. Polym. Sci. Part A Polym. Chem* **2015**, *53*, 2673.
[23] J. Zhang, D. Campolo, F. Dumur, P. Xiao, D. Gigmes, J. P. Fouassier, J. Lalevée, *Polym. Bull* **2016**, *73*, 493.
[24] J. Lalevée, F. Dumur, M. Nechab, D. Gigmes, J. P. Fouassier, *Trends Photochem. Photobiol* **2012**, *14*, 27.
[25] P. Garra, D. Brunel, G. Noirbent, B. Graff, F. Morlet-Savary, C. Dietlin, V. F. Sidorkin, F. Dumur, D. Duché, D. Gigmes, J. P. Fouassier, J. Lalevée, *Polym. Chem* **2019**, *10*, 1431.
[26] H. Chen, G. Noirbent, K. Sun, D. Brunel, D. Gigmes, F. Morlet-Savary, Y. Zhang, S. Liu, P. Xiao, F. Dumur, J. Lalevée, *Polym. Chem* **2020**, *11*, 4647.
[27] R. van Gorkum, E. Bouwman, *Coord. Chem. Rev* **2005**, *249*, 1709.
[28] J. Honzíček, *Ind. Eng. Chem. Res* **2019**, *58*, 12485.
[29] N. Simpson, K. Maaijen, Y. Roelofsen, R. Hage, *Catalysts* **2019**, *9*, 825.
[30] J. W. de Boer, P. V. Wesenhagen, E. C. M. Wenker, K. Maaijen, F. Gol, H. Gibbs, R. Hage, *Eur. J. Inorg. Chem* **2013**, *2013*, 3581
[31] J. Bootsma, W. R. Browne, J. Flapper, B. de Bruin, *JACS Au* **2022**, *2*, 531.
[32] J. Bieleman, T. Bolle, A. Braig, J. K. Glaser, R. Spang, M. Köhler, A. Valet, in *Additives for Coatings*, Vol. *8*, (Ed: J. H. Bieleman), Wiley-VCH **2000**. pp. 257–268. ISBN: 978-3-527-61330-4.
[33] S. Tanase, J. C. Hierso, E. Bouwman, J. Reedijk, J. ter Borg, J. H. Bieleman, A. Schut, *New J. Chem* **2003**, *27*, 854.
[34] M. D. Soucek, T. Khattab, J. Wu, *Prog. Org. Coat* **2012**, *73*, 435.
[35] European Chemicals Agency (ECHA), Substance Information: Cobalt diacetate, https://echa.europa.eu/nl/substance-information/-/substanceinfo/100.028.325. (accessed May 14, 2025).
[36] C. Kohl, C. D. Schiller, A. Gescher, P. B. Farmer, E. Bailey, *Carcinogenesis* **1992**, *13*, 1091.
[37] S. K. Lim, H. S. Shin, K. S. Yoon, S. J. Kwack, Y. M. Um, J. H. Hyeon, H. M. Kwak, J. Y. Kim, T. H. Kim, Y. J. Kim, T. H. Roh, D. S. Lim, M. K. Shin, S. M. Choi, H. S. Kim, B. M. Lee, *Toxicol. Environ. Health, Part A* **2014**, *77*, 1502.
[38] J. L. Schrenk, A. M. McNair, F. B. McCormick, K. R. Mann, *Inorg. Chem* **1986**, *25*, 3501.
[39] A. M. McNair, J. L. Schrenk, K. R. Mann, *Inorg. Chem* **1984**, *23*, 2633.
[40] D. A. Loginov, I. D. Baravi, O. I. Artyushin, Z. A. Starikova, P. V. Petrovskii, A. R. Kudinov, *Russ. Chem. Bull* **2010**, *59*, 1312.
[41] A. G. Abel, R. Lambourne, T. A. Strivens, in *In Paint and Surface Coatings*, (Eds: R. Lambourne, T. A. Strivens), Woodhead Publishing, Sawston, Cambridge **1999**. pp. 91-165. ISBN: 978-1-85573-348-0.
[42] C. Duce, L. Bernazzani, E. Bramanti, A. Spepi, M. P. Colombini, M. R. Tiné, *Polym. Degrad. Stab* **2014**, *105*, 48.
[43] E. Ghelardi, I. Degano, M. P. Colombini, J. Mazurek, M. Schilling, H. Khanjian, T. Learner, *Dyes Pigm.* **2015**, *123*, 396.
[44] N. Sano, P. J. Cumpson, E. Cwiertnia, J. J. Perry, B. W. Singer, *Surf. Interface Anal* **2014**, *46*, 786.
[45] F. C. Izzo, K. J. van den Berg, H. van Keulen, B. Ferriani, E. Zendri, K. J. van den Berg, A. Burnstock, M. de Keijzer, J. Krueger, T. Learner, A. de Tagle, G. Heydenreich, *In Issues in Contemporary Oil Paint*, (Eds: K. J. van den Berg, A. Burnstock, M. de Keijzer, J. Krueger, T. Learner, A. de Tagle, G. Heydenreich), Springer, Cham **2014**. pp. 75–104. ISBN: 978-3-319-10100-2.
[46] E. P. Kündig, P. Jeger, G. Bernardinelli, *Inorganica Chim. Acta* **2004**, *357*, 1909.
[47] E. P. Kündig, *Top. Organomet. Chem.* **2004**, *7*, 3.
[48] E. P. Kündig, P. Jeger, G. Bernardinelli, *Angew. Chem. Int. Ed* **1995**, *34*, 2161.
[49] J. L. Schrenk, M. C. Palazzotto, K. R. Mann, *Inorg. Chem* **1983**, *22*, 4047.
[50] A. N. Nesmeyanov, N. A. Vol'kenau, L. S. Shilovtseva, V. A. Petrakova, *J. Organomet. Chem* **1975**, *85*, 365.
[51] E. Roman, D. Astruc, *Inorg. Chim. Acta* **1979**, *37*, L465.
[52] D. Astruc, *Tetrahedron* **1983**, *39*, 4027.
[53] H. O. Doggweiler, V. Desobry, *Eur. Pat. Appl. EP* **1988**, *270490*.
[54] N. V. Shvydkiy, D. S. Perekalin, *Coord. Chem. Rev* **2020**, *411*, 213238.
[55] E. P. Kündig, C. Perret, S. Spichiger, G. Bernardinelli, *J. Organomet. Chem* **1985**, *286*, 183.
[56] D. A. Loginov, A. A. Chamkin, V. B. Kharitonov, E. R. Sovdagarova, Y. V. Nelyubina, A. R. Kudinov, *ChemistrySelect* **2017**, *2*, 3549.
[57] P. Zanello, R. H. Herber, A. R. Kudinov, M. Corsini, F. F. de Biani, D. A. L. I.Nowik, M. M. Vinogradov, L. S. Shul'pina, I. A. Ivanov, A. V.Vologzhanina, *J. Organomet. Chem.* **2009**, *694*, 1161.
[58] T. P. Gill, K. R. Mann, *Inorg. Chem* **1983**, *22*, 1986.
[59] D. R. Chrisope, K. M. Park, G. B. Schuster, *J. Am. Chem. Soc* **1989**, *111*, 6195.
[60] F. R. van de Voort, A. A. Ismail, J. Sedman, G. Emo, *J. Am. Oil Chem. Soc* **1994**, *71*, 243.
[61] A. S. Sokolov, V. A. Korabelnikova, V. P. Ananikov, D. A. Michurov, V. I. Lozinsky, D. S. Perekalin, *Chem. Commun* **2023**, *59*, 10532.
[62] A. M. Shved, P. A. Zhmurov, E. I. Gutsul, D. S. Perekalin, *New J. Chem* **2020**, *44*, 18157.
[63] B. W. Fitzsimmons, W. G. Marshall, *J. Chem. Soc., Dalton Trans* **1992**, 73. https://pubs.rsc.org/en/content/articlelanding/1992/dt/dt9920000073.
[64] K. Ôno, A. Ito, *J. Phys. Soc. Jpn* **1964**, *19*, 899.
[65] R. W. Grant, H. Wiedersich, A. H. Muir Jr., U. Gonser, W. N. Delgass, *J. Chem. Phys* **1966**, *45*, 1015.
[66] N. Chen, Y. Zhao, M. Li, X. Wang, X. Peng, H. Sun, L. Zhang, *J. Hazard. Mater* **2022**, *436*, 129049.
[67] V. A. Varnek, I. K. Igumenov, P. A. Stabnikov, L. N. Mazalov, *J. Struct. Chem* **2000**, *41*, 977.
[68] M. Pápai, G. Vankó, *J. Chem. Theory Comput* **2013**, *9*, 5004.
[69] H. Ahouari, G. Rousse, J. Rodríguez-Carvajal, M.-T. Sougrati, M. Saubanère, M. Courty, N. Recham, J.-M. Tarascon, *Chem. Mater* **2015**, *27*, 1631.

Manuscript received: April 11, 2025
Revised manuscript received: June 18, 2025
Version of record online: